Article:
Chudpooti, N, Doychinov, V orcid.org/0000-0001-6730-0057, Hong, B orcid.org/0000-0002-8033-5438 et al. (3 more authors) (2018) Multi-modal millimeter-wave sensors for plastic polymer material characterization. Journal of Physics D: Applied Physics, 51 (27). 275103. ISSN 0022-3727

https://doi.org/10.1088/1361-6463/aac818

Multi-Modal Millimeter-Wave Sensors for Plastic Polymer Material Characterization

Multi-modal millimeter-wave sensors for plastic polymer material characterization

N Chudpooti[1], V Doychinov[2], B Hong[2], P Akkaraekthalin[1], I Robertson[2] and N Somjit[2]

[1] Department of Electrical and Computer Engineering, Faculty of Engineering,
King Mongkut's University of Technology North Bangkok, Bangkok, 10800, Thailand
[2] School of Electronics and Electrical Engineering, University of Leeds, Leeds, LS2 9JT, U.K.

Email: c.nonchanutt@gmail.com

Abstract

This paper presents, for the first time, a multimodal sensor for characterizing relative permittivity of plastic polymers by integrating in a single sensor (1) frequency-reconfigurable resonance technique at 98 and 100 GHz, and (2) 80-100-GHz broadband modified transmission-line technique. The sensor is designed based on a custom-made WR-10 waveguide featuring dual rectangular Complementary Split-Ring Resonators (CSRRs). By loading the CSRRs with a Material-Under-Test (MUT), the reflected and transmitted electromagnetic waves propagating inside the waveguide are changed depending on the dielectric properties of the material. Various plastic polymer materials, e.g. Polytetrafluoroethylene (PTFE), Polymethylmethacrylate (PMMA) and High-Density Polyethylene (HDPE), are characterized. The sensor in this paper offers various key advantages over any state-of-the-art material characterization techniques at millimeter-wave frequencies, e.g. multiple characterization techniques integrated in a single device, miniaturization, much higher tolerance to changes in the measurement environment, ease of design and fabrication, and better cost effectiveness.

Keywords: Complex dielectric properties, millimeter-wave, CSRR, modified transmission-line, microwave measurements

1. Introduction

There are several techniques for characterizing dielectric material properties, such as relative permittivity and loss tangent, at the RF and microwave spectrum. In recent years, a lot of research activities [1-22] have been aiming at improving the accuracy and sensitivity of material characterization, especially at frequencies below 50 GHz [1-17]. However, very few contributions attempt to characterize dielectric and semiconductor materials at the millimeter-wave and THz frequency bands [18-22], [27], which are becoming increasingly important in various applications in sciences and engineering. Even so, there are currently only six commercial material characterization techniques available to date [1-17] and only two of which are suitable at the frequencies above 50 GHz.

A coaxial probe [1-5] is frequently used to characterize both solid and liquid materials, since it requires only a simple one port measurement. However, the use of this technique is limited to 50 GHz due to the physical size of the probe and suitable only for large volume or large size material samples. The parallel plate capacitor [13-16] and toroidal-core inductance techniques [17] involve lumped element components to evaluate the properties of the Material-Under-Test (MUT), and are thus suitable for use only at very low frequencies, normally below 10 GHz [1]. The resonance cavity method [10-12] on the other hand is generally used to characterize materials with the most accurate dielectric properties at a single frequency and is unsuitable for characterizing high-loss materials due to the broadening of the resonance peak as the material loss increases. Furthermore, at high frequencies above 50 GHz the size of the resonance cavity becomes very small, making MUT sample preparation and cavity fabrication difficult.

At frequencies above 50 GHz, the free-space technique [1] is commonly used in commercial material characterization systems. The main disadvantage of this technique is that the measurement is performed in free space, resulting in various uncertainties introduced by open measurement environments, which can drastically decrease the characterization accuracy. The free-space technique is also bulky and complicated to setup, requiring experienced personnel to establish accurate

and well-controlled measurement environments. The conventional transmission-line technique [6-9], using an MUT sample placed inside a hollow rectangular metal waveguide, is a broadband characterization method operating up to 1.1 THz [1-18], [27], covering both low-loss and high-loss materials. However, above millimeter-wave frequencies, the size of the waveguide becomes very small, complicating the MUT sample preparation and measurement setup, since the MUT must be inserted fully inside the hollow waveguide.

Overall, few research results have been published on dielectric material property characterization at millimeter-wave and THz frequencies [18-22], [27]. These techniques include laminated waveguide [18], time-domain measurements [19], [22], microstrip ring resonators [20], and Frequency Selective Surface (FSS) filters [21]. Main key disadvantages of these methods include complicated setup (time domain), as well as design and fabrication complexities and costs, for examples laminated waveguide and ring resonator.

In this paper, we present a miniaturized waveguide-based sensor for characterizing the relative permittivity of materials, e.g. plastic polymer materials, integrating two measurement methods in a single device. The sensor is designed to operate within the 75-110 GHz WR-10 waveguide band featuring Complementary Split Ring Resonators (CSRRs). The other higher frequency bands can be covered by simple scaling of its physical dimensions. The key advantages of the proposed sensor are that it combines: (1) frequency reconfigurable resonance technique at 98 and 100 GHz by using a sliding short-circuit component, which is used to extend the capability of the measurement to multiple discrete frequency points; (2) 80-100-GHz broadband modified transmission-line technique, which is particularly useful for characterizing high-loss materials e.g. liquid and highly-doped semiconductors; (3) ability to quickly switch between these two measurement modes depending on user requirements, i.e. high-accuracy single-frequency measurements or broadband characterization; and (4) ease of operation, as the MUT sample is placed on top of the CSRRs, rather than inserted inside the waveguide, which also reduces the sample preparation complexity. Software packages developed with Origin by the authors together with simulations performed in CST Studio Suite are used to extract the relative permittivity of the MUT from measured S-parameter data. In this paper, material measurements and extracted dielectric parameters for PTFE, HDPE, and PMMA are presented, which are common materials for additive manufacturing etc. The choices of materials are only limited by the material available in our laboratory, not by the sensor capability. The extracted results show an average agreement in relative permittivity of higher than 92% compared to free-space measurement results. The sensor in this paper offers various key advantages over any state-of-the-art material characterization techniques at millimeter-wave, e.g. multiple characterization techniques integrated in a single device, miniaturization, frequency-reconfigurability for wider functional material characterization, much higher tolerance to changes in the measurement environment, ease of design and fabrication, and better cost effectiveness.

2. Sensor description and design

The design of the sensor utilizes a custom-designed H-plane split WR-10 waveguide block, with integrated dual CSRRs into the top wall of the waveguide. An annotated view of the sensor before assembly is shown in figure 1(a) while figure 1(b) shows the device after assembly.

The fundamental operating principle of the sensor is the same for both the resonance and transmission line characterization techniques, both of which are used to design the sensor in this work. Each characterization technique offers

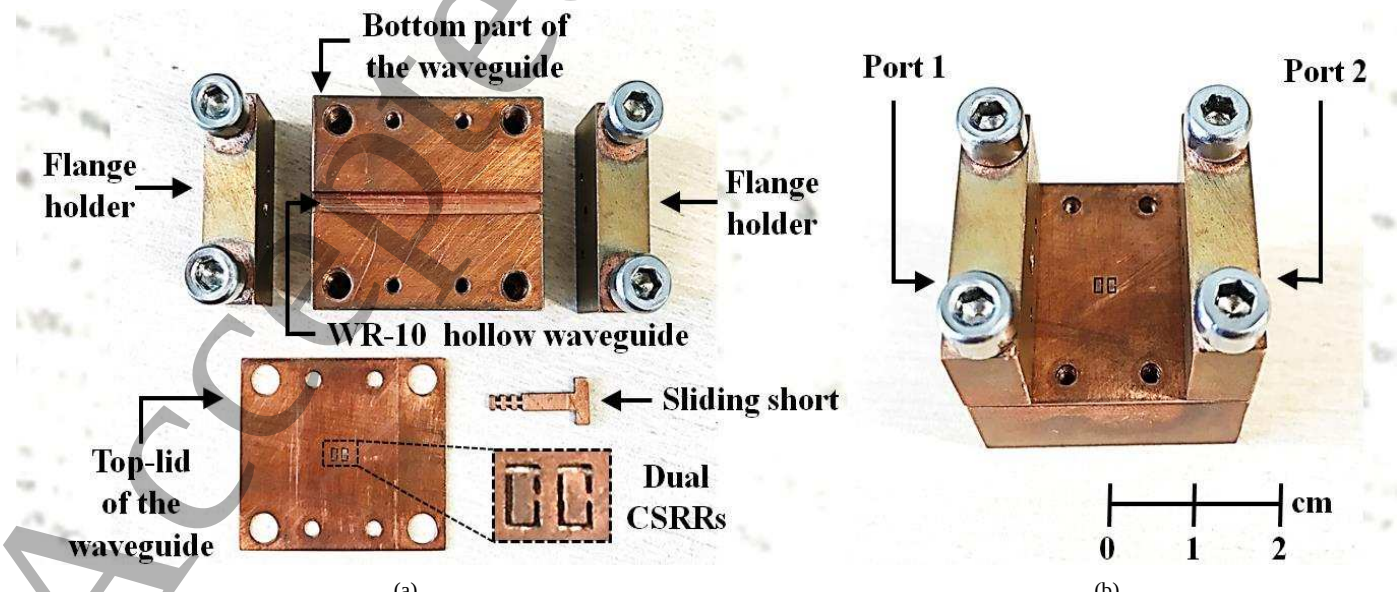

(a) (b)

Figure 1. (a) Fabricated sensor prototype before assembly, which consists of the bottom of the waveguide, an integrated dual CSRRs embedded into the top wall of the waveguide, two flange holders, and the sliding short-circuit component, and (b) fabricated instrument prototype after assembly.

different advantages and is suitable for different scenarios, e.g. the resonance technique is preferred for high-accuracy single frequency measurements, whereas the modified transmission-line technique is used for broadband material characterization. For both techniques, electromagnetic (EM) energy in the form of guided propagating EM waves is coupled into the waveguide hollow at Port 1, as shown in figure 1(b), and interacts with the MUT via the dual CSRRs. This interaction, depending on the dielectric properties of the material, affects the amount of energy reflected back to Port 1 and transmitted to Port 2 and can be quantified using the S-parameters S_{11} and S_{21}, respectively. The material properties, i.e. relative permittivity and loss tangent, can then be determined through the mathematical models presented in section 3.

The CSRRs are designed in the middle of the broad wall of the waveguide, where the electric field is at a maximum [29], resulting in measurement results with the best possible accuracy and sensitivity. Dual CSRRs are used to further increase the coupling interactions between the electric field radiated from the resonators and the MUT, as the sample to be measured is mounted on top of the CSRRs fabricated into the top-lid sheet. figure 2(a) shows a top-view drawing of the dual CSRRs, while figure. 2(b) presents their lumped-element equivalent circuit. The capacitance, denoted by C_{C1} and C_{C2}, is due to the slots etched into the top sheet, and is dependent on their width and overall length. The inductance, contributed by L_{C1} and L_{C2}, is determined by the size of the metal strip connecting the inner metal patches to the rest of the sheet, given by g and w. Finally, the inductor L_{C3} and capacitor C_{C3} represent the mutual coupling between the two resonators. The values of total capacitance loading the line, C_C, and total inductance loading the line, L_C, determine the resonant frequency [23]. The dimensions of the CSRRs were optimized using 3D EM simulation to design the nominal resonant frequency of the unloaded CSRRs within the WR-10 frequency band. The optimum values of all design parameters shown in figure 2(a) are listed in table 1.

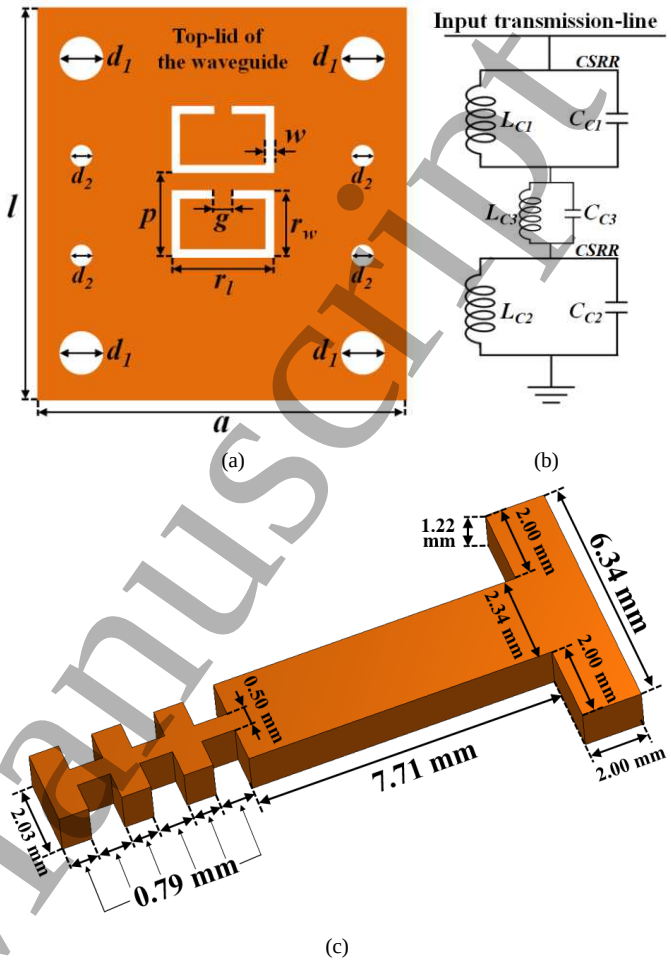

Figure 2. (a) 2D drawing of the top conductor wall of the waveguide with dual CSRRs and (b) the equivalent circuit model of the two CSRRs embedded into the top wall of the waveguide, and (c) 3D drawing of sliding short-circuit component.

Table 1. Summary of the design parameters

Parameter	Description	Length (mm)
a	Waveguide width	2.54
d_1	Diameter for locking flange holders	4.00
d2	Diameter for locking MUT	2.00
g	Gap width	0.23
l	Waveguide length	30.0
p	Pitch	1.50
r_l	Ring length	1.81
r_w	Ring width	1.00
w	Slot width	0.17

2.1. Resonance functionality design

To perform material characterization with the resonance technique, a sliding short-circuit component is inserted at one of the waveguide ports, resulting in one-port signal-reflection measurements as shown in figure 3(a) and 3(b). The distance between the CSRRs and the tip edge of the sliding short is $3\lambda_g/4$ where λ_g is the wavelength of the EM signal propagating inside the waveguide at the nominal frequency of 100 GHz. The total length of the sliding short-circuit component is 12.45 mm. In the nominal case, when the sliding short-circuit structure is fully inserted, a minimum in the S_{11} is observed at a particular frequency, approximately at 100 GHz in this instance. That frequency is referred to as the nominal resonant frequency and is denoted as f_r in this work. The nominal resonant frequency can be tuned by adjusting the distance of the sliding short-circuit inserted inside the waveguide. When an MUT sample is placed on top of the CSRRs, both the magnitude of S_{11} and the frequency f_r change, depending on the dielectric properties of the MUT.

The requirement for implementing a sliding short-circuit component is that it must be fabricated from a single low-loss metal blank and is able to come into direct contact with the waveguide walls, resulting in a high quality short circuit, without introducing any additional EM signal losses. The sliding short-circuit component was designed as a series of alternating low-impedance and high-impedance sections, spaced at $\lambda_g/4$, achieving high quality short circuit termination [24]. A 3D model of the sliding short-circuit component is

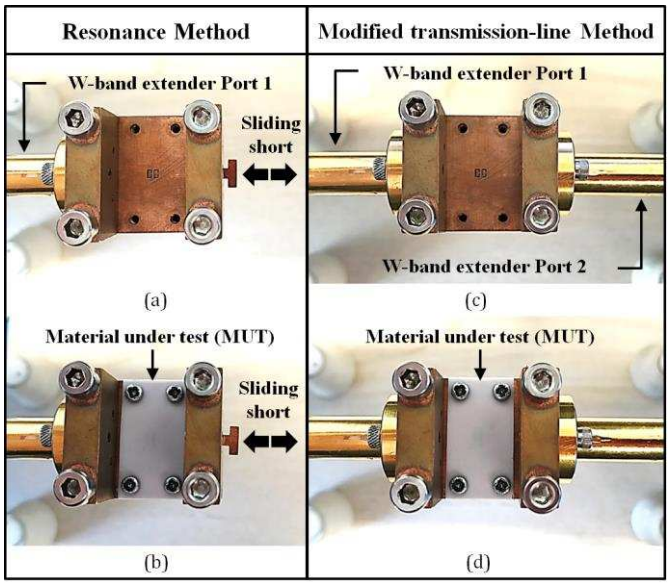

Figure 3. (a) Resonance measurement setup, Port 1 is connected to the network analyzer through a W-band extender and Port 2 is terminated with sliding short-circuit component for adjusting resonant frequencies, (c) modified transmission-line measurement setup, both sides of the sensor connect to W-band extenders, (b) and (d) the MUT is placed and secured with M2 screws on top of the sensor during measurement of resonant and transmission-line techniques, respectively.

shown in figure 2(c), together with its dimensions. Furthermore, from the measurement results, the sliding short-circuit component does not need to be in full contact with all walls of the waveguide to perform a good short-circuit termination, only the bottom broad wall is sufficient [24].

2.2. Modified transmission-line functionality design

Broadband modified transmission-line functionality is implemented by removing the contacting sliding short-circuit component from the measurement setup, turning the waveguide into a full two-port device, as shown in figure 3(c) and figure 3(d). Similar to the resonance functionality, the CSRRs are loaded with the MUT on top of the top lid. The dimensions of the waveguide channel are standard WR-10 ones, i.e. 2.54 mm × 1.27 mm, thereby ensuring good impedance match with the measurement system. Unlike the resonance technique, only the magnitude of the S_{21} is of interest for this method. There are two main advantages of the transmission-line method modification in this work, i.e. placing the MUT on top of the CSRRs rather than inside the waveguide. Normally, in conventional transmission line measurements, the EM signal is heavily absorbed in the MUT sample, especially in the case of millimeter-wave frequencies and high-loss materials leading to poor characterization results, as very little energy reaches Port 2. The other benefit of mounting the sample on top of the CSRRs is the ease of MUT sample preparation, as the MUT sample is placed on top of the waveguide, rather than inserted inside it, which also reduces the sample preparation complexity.

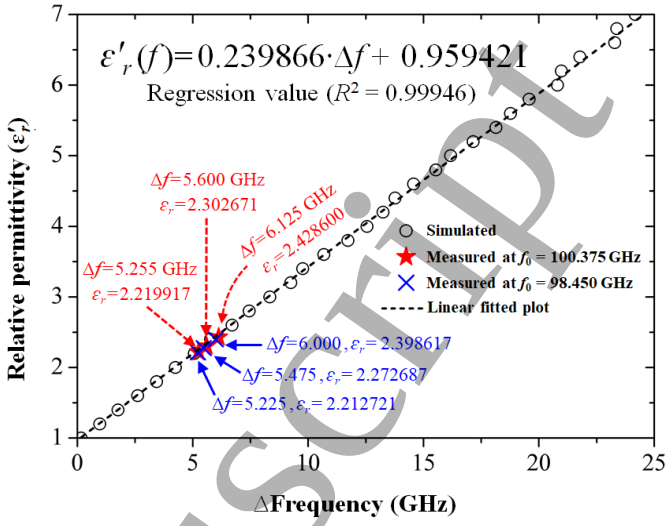

Figure 4. Linear fitted curve for determination of relative permittivity as a function of resonant frequency change (Δf_r) in GHz. The regression value and the linear fitted (dash line), as calculated by Origin, are also annotated. The measured results are denoted by an "X" symbol and correspond to the measured values of relative permittivity presented in table 2 and 3.

2.3. Sensor fabrication and assembly

The individual constituent parts of the sensor were shown in figure 1(a) and were fabricated using a variety of methods in the EPSRC National Facility for Innovative Robotic Systems at the University of Leeds.

The bottom half, which contains the full-sized WR-10 waveguide channel, is machined out of a single copper block using a 5-axis CNC milling machine. The bottom half also has four tapped holes for attaching the upper flange structures and the top lid sheet using fastening screws.

The top lid of the waveguide is fabricated out of a 0.5-mm thick copper sheet, with the CSRRs etched into it by using LPKF ProtoLaser U3. Implementing the sensor with this approach provides customization options, by allowing different top lid sheets with different resonator structures to be used and fabricated separately from the bottom waveguide structure.

The terminating sliding short-circuit component was also structured using LPKF ProtoLaser U3, and the two flange holders, which are mounted on both ends of the sensor, were fabricated from two smaller copper blocks.

To fully assemble the sensor, as presented in figure 1(b), M4 screws are used to fasten and secure the top half and the flange holders to the bottom half, minimizing gaps in the H-plane and ensuring good EM performance. At the same time, a standard UG-387/U-M flange [28] is implemented, to ensure correct mating with laboratory measurement equipment. Prior to the material measurement, an MUT sample with dimensions of 26 mm × 14 mm, with 2 mm diameter holes drilled at its four corners, must be prepared. Then, the MUT is mechanically secured on top of the CSRRs using M2 screws, resulting in the absence of an air gap between the MUT and CSRRs.

3. Relative permittivity extraction model

3.1. Sensor design optimization

The initial sensor design was generated using the commercially available 3D EM simulation tool CST Studio Suite, which is based on the Finite Element Method (FEM). The values of all design parameters of CSRR are listed in table 1, given for an operating frequency of 100 GHz. After assembly, the measured results of the reflection coefficient (S_{11}) showed that the operating frequency f_r had shifted to 100.375 GHz, which was attributed to dimension tolerances and inaccuracies from the manufacturing processes. The actual dimensions of the fabricated sensor were measured under high magnification optical microscope to obtain better matching between simulation and measurement results.

3.2. Resonance technique

To develop the numerical model for the extraction of the materials' relative permittivity from the S-parameter measurements, a preliminary analysis was carried out in silico using the 3D EM simulator CST Studio Suite. The entire sensor assembly, as illustrated in figure 3(b), was modelled, including an MUT sample. The sample was represented in CST as a rectangular box with the same dimensions as the physical samples available. A parametric sweep was then used to vary the real part of the relative permittivity ε'_r of the modelled MUT. The values used were 1 to 7 in steps of 0.2 for ε'_r. For each of the resulting 31 simulations, the new, shifted resonant frequency in the reflection coefficient (S_{11}) was recorded. The amount by which the resonant frequency has shifted away from 100.375 GHz, Δf_r, is then calculated and plotted as a function of the relative permittivity in figure 4.

These individual data points were then fitted into to a line using the commercially available data analysis and visualization software package, Origin, where the linearly fitted plot was found to offer the best fit with a regression value R^2 of 0.99946. The fit is given as:

$$\varepsilon'_r(f) = 0.239866 \cdot \Delta f + 0.959421 \quad (1)$$

where $\varepsilon'_r(f)$ is the relative permittivity as a function of the change in resonant frequency Δf_r GHz as a function of loading the CSRR with an MUT. A comparison between the fitted and measured values is also shown in figure 4. Equation (1) can now be used to determine the relative permittivity of samples.

3.3. Modified transmission-line technique

For the modified transmission-line technique, the sliding short-circuit was removed from the measurement setup, thereby creating a full two-port device for broadband material characterization. The same materials as with the resonance method were measured, namely PTFE, HDPE and PMMA. The analysis of this characterization method requires two reference S-parameter measurements to obtain an accurate model. The full measurement and analysis procedure consists of the following steps:

1. Measure the full 2-port S-parameters without any MUT sample loading the CSRRs, i.e. air, as the reference measurement.
2. Measure the full 2-port S-parameters with the MUT securely placed on top of the CSRRs as the second reference measurement.
3. Accurately modified transmission-line technique, the physical dimensions of the sensor and MUTs are modelled in CST Studio Suite and optimize the value of its relative permittivity until simulated frequency response match with measured S_{21} results.

When the simulation match with measurement results, the dielectric property of the MUT is extracted.

4. Measurement results

To measure the S-parameters for different MUTs, Keysight Technologies PNA-X N5242A with OML WR-10 VNA Extender Heads was used. Prior to performing any measurements, the Thru-Reflect-Line (TRL) calibration method was used to eliminate the systematic errors contributed by the PNA-X, connecting cables, and the Extender Heads. For both setups, the measurements were achieved over the entire WR-10 frequency range, i.e.75 GHz – 110 GHz. The S-parameter measurements were performed in an environment with controlled low humidity and maintained at a temperature of 24 °C. Individual measurements were repeated three times to ensure repeatability. The averages were subsequently used to extract the dielectric properties of the materials. Results obtained using the Keysight Technologies free space material characterization suite 85071E [26] were used for comparison and validation purposes.

4.1. Resonance technique

The measured $|S_{11}|$ of commercially available polymer materials, i.e., PTFE [37], HDPE [38], PMMA [39], and air, used as a reference material, are shown in figure 5(a) when the sliding short-circuit component was fully inserted into the waveguide, and in figure 5(b) when the position of the short-circuit component inside the waveguide was changed to tune the nominal resonant frequency to 98 GHz. As described, loading the CSRRs with an MUT sample causes the resonant frequency to shift downwards and the return loss to increase. The amount by which the frequency shifts and magnitude of S11 changes relate to the relative permittivity of the MUT. A larger shift in the resonant frequency is observed for a material with higher relative permittivity.

Using equation (1), the permittivity of the MUT is extracted from the measured data in the following way:

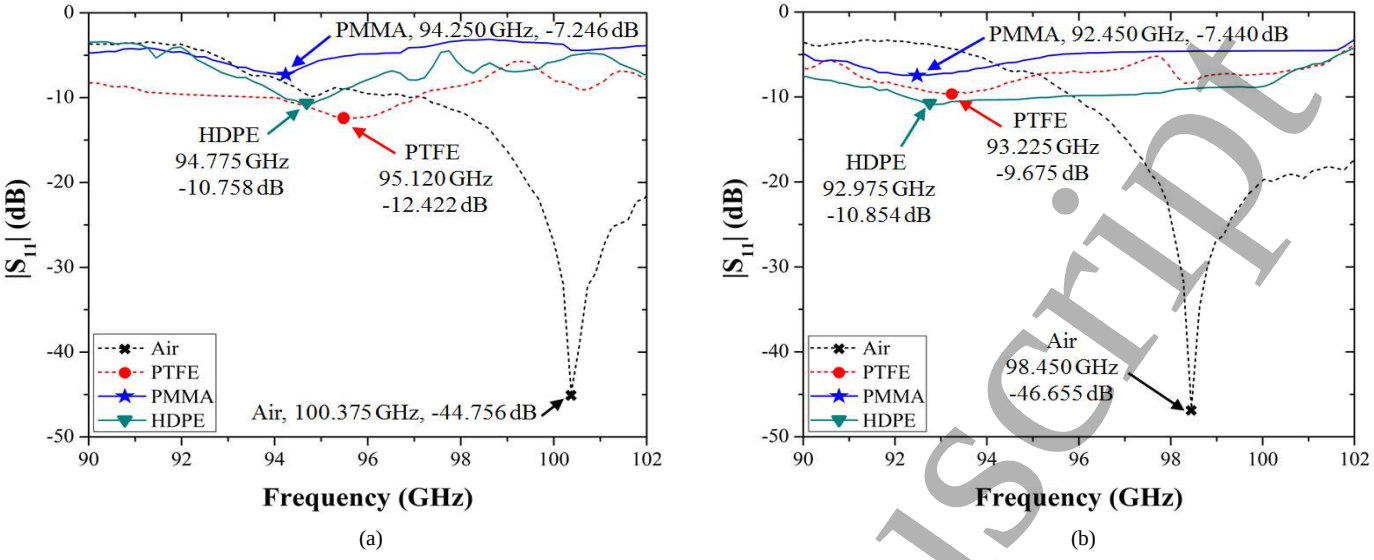

Figure 5. Measured S_{11} results of PTFE, PMMA and HDPE samples (a) operating frequency before placing the MUT at 100.375 GHz and (b) after tuning the position of the sliding short-circuit component in the waveguide, which resulted in a change of the resonant frequency to 98.450 GHz.

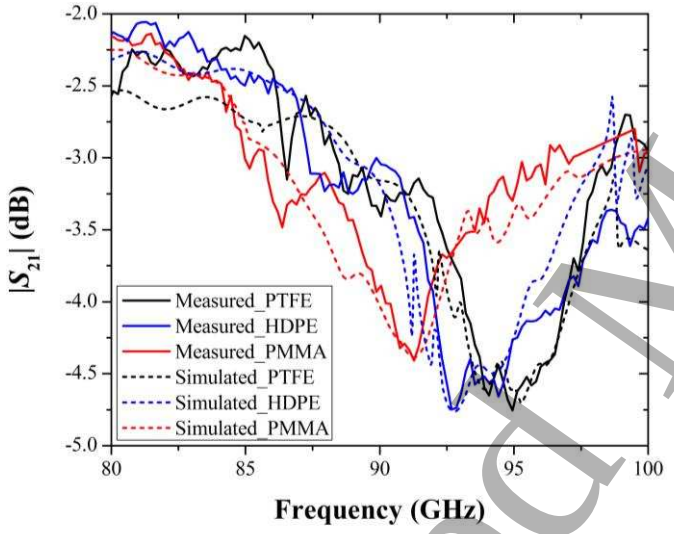

Figure 6. Simulated (dashed line) and measured (solid line) $|S_{21}|$ results, for loaded three MUTs, i.e. PTFE, HDPE, and PMMA.

1. Measure the air standard and record the resonant frequency and S_{11}.
2. Measure the MUT sample and calculate the resonant frequency change from $|\Delta f| = | f_r - f_{MUT} |$
3. Use equation (1) to calculate the relative permittivity ε'_r.

The extracted relative permittivity values are presented in table 2 for the case of a fully inserted sliding short-circuit component and are compared with the values measured by using the Keysight free-space measurement suite 85071E for certain frequency points of interest.

From table 2, it is evident that the sensor developed in this work has a good accuracy when compared with the commercial free-space solution. The largest difference in relative permittivity between the two methods was only 8.03%. The extracted values of the relative permittivity from the three materials were also more consistent than the laser source free space measurement, which yielded a negative value for the loss tangent of the materials-under-test.

Table 2. Resonance technique relative permittivity extraction results of three materials (operating frequency at 100.375 GHz).

Material Under Test (MUT)	Resonance frequency (GHz)	Resonant method (**this work**) ε'_r	Keysight free space measurement ε'_r	Difference ratio $\Delta\varepsilon'_r / \varepsilon'_r$
PTFE	95.120	2.2199	2.0550	0.0803
HDPE	94.775	2.3026	2.3675	0.0273
PMMA	94.250	2.4286	2.6115	0.0700

Table 3. Resonance technique relative permittivity extraction results of three materials (operating frequency at 98.450 GHz).

Material Under Test (MUT)	Resonance frequency (GHz)	Resonant method (**this work**) ε'_r	Keysight free space measurement ε'_r	Difference ratio $\Delta\varepsilon'_r / \varepsilon'_r$
PTFE	93.225	2.2127	2.0577	0.0754
HDPE	92.975	2.2727	2.3668	0.0398
PMMA	92.450	2.3986	2.6100	0.0809

Table 4. Modified transmission-line technique relative permittivity extraction results of three materials.

Material Under Test (MUT)	Modified transmission line method (**this work**) ε'_r	Keysight free space measurement ε'_r	Difference ratio $\Delta\varepsilon'_r / \varepsilon'_r$
PTFE	2.11	2.0550	0.0268
HDPE	2.32	2.3675	0.0201
PMMA	2.57	2.6115	0.0159

4.2. Resonance technique: tuning capability

The tuning capability of the sensor is demonstrated by moving the sliding short-circuit component to a different position inside the waveguide, designed for optimal EM energy coupling between the waveguide and the MUT through the

Table 5. Relative permittivity comparison of measurement of this work and other works

Material Under Test (MUT)	Resonant method at 100.375 GHz (**this work**)	Resonant method at 98.450 GHz (**this work**)	Modified transmission line method at 80 –100 GHz (**this work**)	Keysight free space measurement at 100 GHz	[31] at 100 GHz	[32] at 100 GHz	[33] at 350 – 500 GHz	[34] at 100 GHz	[35] at 100 GHz	[36] at 150 GHz
PTFE	2.2199	2.2127	2.11	2.0550	2.0303	2.02	2.02-2.04	2.07	2.0701	2.0535
HDPE	2.3026	2.2727	2.32	2.3675	2.2129	2.29	N/A	N/A	N/A	2.3244
PMMA	2.4286	2.3986	2.57	2.6115	2.6016	N/A	2.58-2.61	2.46	2.585	2.5887

CSRRs, allowing characterization of the relative permittivity of the MUT at a different frequency point of interest.

In section 4, the sliding short-circuit component was fully inserted into the waveguide at 12.45 mm length from Port 2. Thereafter, the sliding short-circuit component was inserted into the waveguide up to 10.78 mm from Port 2 to obtain another maximum coupling point, hence, changing the nominal frequency to 98.45 GHz. The measured results of the three MUT samples are shown in figure 5(b). The extracted relative permittivity values are compared with the values measured using Keysight 85071E and are shown in table 3. The extracted results for this new frequency point again show good accuracy when compared with the commercial free-space method, with the biggest difference in relative permittivity between the two methods being only 8.09%. This shows that the sensor retains the high accuracy offered by the resonance technique after tuning the measurement frequency, making it relevant for cases where the relative permittivity of material is required at a specific frequency point.

4.3. Modified Transmission-line technique

The modified transmission-line characterization setup was illustrated in figure 3(c) and 3(d). The measured S_{21} for the same three MUTs as in the resonance characterization technique, i.e. PTFE, HDPE, PMMA, together with the air standard are shown in figure 6.

The values for the relative permittivity of PTFE, PMMA and HDPE over the mentioned frequency band were extracted following steps in section 3.3. The relative permittivity of three material are compared to the results from the Keysight free space method as shown in table 4. There is good agreement between the proposed sensor and the free-space probe. The biggest difference in relative permittivity between the two methods was only 2.68%.

Unlike the resonance method, which was used to measure the relative permittivity of the different MUT at specific discrete frequency points, the modified transmission-line technique is used to characterize these properties over a finite bandwidth. Therefore, a different metric is needed to quantify the performance of the sensor.

The extracted results of relative permittivity of plastic polymer materials, e.g. PTFE, HDPE, and PMMA, which were measured using proposed method are listed in table 5. Furthermore, the results of earlier studies were included in this table to compare the relative permittivity of the three polymer materials. In table 5, the extracted relative permittivity shows a good agreement when compared with previous works [31-36]. The different frequency bands at which data for the permittivity of the three materials investigated in this work were available are also for completeness and to demonstrate the similarity in results between this work and previous publications. The compared results show that both proposed measurement techniques are suitable to relative permittivity measurement of bulk solid samples at W-band frequencies.

4.4. Repeatability performance of the sensor

To measure the repeatability of the sensor, two experiments were performed. Firstly, the MUTs are mechanically remounted three times, and the standard deviation of these measurements is calculated. The maximum of that over the entire frequency band for the resonance, tuned resonance and modified transmission-line technique are 0.653243, 0.699002, and 0.222502, respectively. Secondly, the proposed sensor is taken out and re-mounted during measurement, the results of the standard deviation of the resonance, tuning resonance and modified transmission-line technique are 0.539824, 0.549886, and 0.24609, respectively.

5. Conclusion

Multimodal sensors for characterization of relative permittivity of materials at millimeter-wave frequencies have been proposed and its performance investigated in this work. Two major modes of operation of the sensor are identified and described. The first one, resonance mode, gives highly accurate results at a single frequency point, and provides quick indication of the properties of the MUT with a better than 92% accuracy when compared to a commercially available solution. The second one, modified transmission-line mode, provides measurement results over a wider frequency range, resulting in a broadband characterization of the MUT. Furthermore, by adjusting the position of one of the sensor's components, it offers tuning functionality when operated in resonance mode. This way, the sensor is able to offer the accuracy of the resonance mode at a different frequency point of interest. The sensor can be reused without degradation or life cycle limitation.

Acknowledgments

This work has been supported by the Engineering and Physical Sciences Research Council (EPSRC) under Grant EP/N010523/1, the Thailand Research Fund through the TRF Senior Research Scholar Program with Grant No. RTA6080008 and the Royal Golden Jubilee Ph.D. Program with Grant No. PHD/0093/2557.

References

[1] Keysight Technologies. (2017, Mar 7). Basics of measuring the dielectric properties of materials – Application note [online]. Available: http://literature.cdn.keysight.com/litweb/pdf/5989-2589EN.pdf.

[2] Y. Xu, R. Bosisio, A. Bonincontro, F. Pedone and G. F. Mariutti, "On the measurement of microwave permittivity of biological samples using needle-type coaxial probes," IEEE Trans. Instrum. Meas., vol. 42, no. 4, pp. 822-827, Aug. 1993.

[3] Y. Xu, F. M. Ghannouchi and R. G. Bosisio, "Theoretical and experimental study of measurement of microwave permittivity using open ended elliptical coaxial probes," IEEE Trans. Microw. Theory Tech., vol. 40, no. 1, pp. 143-150, Jan 1992.

[4] P. M. Meaney, A. P. Gregory, J. Seppälä and T. Lahtinen, "Open-Ended Coaxial Dielectric Probe Effective Penetration Depth Determination," IEEE Trans. Microw. Theory Tech., vol. 64, no. 3, pp. 915-923, Mar. 2016.

[5] S. A. Komarov, A. S. Komarov, D. G. Barber, M. J. L. Lemes and S. Rysgaard, "Open-Ended Coaxial Probe Technique for Dielectric Spectroscopy of Artificially Grown Sea Ice," IEEE Trans. Geoscience Remote Sensing, vol. 54, no. 8, pp. 4941-4951, Aug. 2016.

[6] R. A. Court, "Determination of the Parameters of Microwave Transmission Lines from Transmission and Reflection Measurements," IEEE Trans. Instrum. Meas., vol. 26, no. 4, pp. 419-420, Dec. 1977.

[7] J. C. Booth, N. D. Orloff and J. Mateu, "Measurement of the Microwave Nonlinear Response of Combined Ferroelectric-Superconductor Transmission Lines," IEEE Trans. Appl. Superconductivity, vol. 19, no. 3, pp. 940-943, Jun. 2009.

[8] D. A. Houtz, D. Gu and D. K. Walker, "An Improved Two-Port Transmission Line Permittivity and Permeability Determination Method with Shorted Sample," IEEE Trans. Microw. Theory Tech., vol. 64, no. 11, pp. 3820-3827, Nov. 2016.

[9] N. Meyne née Haase, G. Fuge, H. K. Trieu, A. P. Zeng and A. F. Jacob, "Miniaturized Transmission-Line Sensor for Broadband Dielectric Characterization of Biological Liquids and Cell Suspensions," IEEE Trans. Microw. Theory Tech., vol. 63, no. 10, pp. 3026-3033, Oct. 2015.

[10] S. Corbellini and R. M. Gavioso, "A Low-Cost Sensor for the Accurate Measurement of Resonances in Microwave Cavities," IEEE Trans. Instrum. Meas., vol. 62, no. 5, pp. 1259-1266, May 2013.

[11] A. J. Canos, J. M. Catala-Civera, F. L. Penaranda-Foix and E. Reyes-Davo, "A novel technique for deembedding the unloaded resonance frequency from measurements of microwave cavities," IEEE Trans. Microw. Theory Tech., vol. 54, no. 8, pp. 3407-3416, Aug. 2006.

[12] M. Martinelli, P. A. Rolla and E. Tombari, "A Method for Dielectric Loss Measurements by a Microwave Cavity in Fixed Resonance Condition," IEEE Trans. Microw. Theory Tech., vol. 33, no. 9, pp. 779-783, Sep. 1985.

[13] Y. Shi, M. Zhou and J. Zhang, "Parallel Plate Mode Suppression in Low-Frequency Microwave Circuit Packages Using Lid of 3-D Cross by a 3-D Printing Technique," IEEE Trans. Electromagnetic Compatibility, vol. 59, no. 4, pp. 1268-1271, Aug. 2017.

[14] I. Vakili, M. Gustafsson, D. Sjöberg, R. Seviour, M. Nilsson and S. Nordebo, "Sum Rules for Parallel-Plate Waveguides: Experimental Results and Theory," IEEE Trans. Microw. Theory Tech., vol. 62, no. 11, pp. 2574-2582, Nov. 2014.

[15] L. Anderson, S. S. Stuchly and G. B. Gajda, "Parallel-plate coaxial sensor for dielectric measurements — Further analysis," IEEE Trans Instrum Meas, vol. IM-35, no. 1, pp. 89-91, Mar. 1986.

[16] A. P. Mourachkine and A. R. F. Barel, "Microwave measurement of surface resistance by the parallel-plate dielectric resonator method," IEEE Trans. Microw. Theory Tech., vol. 43, no. 3, pp. 544-551, Mar. 1995.

[17] K. K. Davis et al., "Proof-of-Concept Demonstration of Vector Beam Pattern Measurements of Kinetic Inductance Detectors," IEEE Trans. Terahertz Sci. Technology, vol. 7, no. 1, pp. 98-106, Jan. 2017.

[18] X. Wang and A. Stelzer, "Millimeter-Wave Material Characterization Using Laminated Waveguides," IEEE Trans. Microw. Theory Tech., vol. 62, no. 8, pp. 1762-1771, Aug. 2014.

[19] I. Vakili, L. Ohlsson, L. E. Wernersson and M. Gustafsson, "Time-Domain System for Millimeter-Wave Material Characterization," IEEE Trans. Microw. Theory Tech., vol. 63, no. 9, pp. 2915-2922, Sep. 2015.

[20] R. G. Pierce, R. Islam, R. M. Henderson and A. Blanchard, "SU-8 2000 Millimeter Wave Material Characterization," IEEE Microw. Wireless Components Lett., vol. 24, no. 6, pp. 427-429, Jun. 2014.

[21] O. Sushko, M. Pigeon, R. S. Donnan, T. Kreouzis, C. G. Parini and R. Dubrovka, "Comparative Study of Sub-THz FSS Filters Fabricated by Inkjet Printing, Microprecision Material Printing, and Photolithography," IEEE Trans. Terahertz Sci. Technology, vol. 7, no. 2, pp. 184-190, Mar. 2017.

[22] J. A. Hejase, E. J. Rothwell and P. Chahal, "A Multiple Angle Method for THz Time-Domain Material Characterization," IEEE Trans. Terahertz Sci. Technology, vol. 3, no. 5, pp. 656-665, Sep. 2013.

[23] A. Ebrahimi, W. Withayachumnankul, S. F. Al-Sarawi and D. Abbott, "Compact Dual-Mode Wideband Filter Based on Complementary Split-Ring Resonator," IEEE Microw. Wireless Components Lett., vol. 24, no. 3, pp. 152-154, Mar. 2014.

[24] J. R. Stanec, and N. S. Barker, "A Rectangular-Waveguide Contacting Sliding Short for Terahertz Frequency Applications," IEEE Trans. Microw. Theory Tech., vol. 61, no. 4, pp. 1488-1495, Apr. 2013.

[25] T. Chretiennot, D. Dubuc, and K. Grenier, "A microwave and microfluidic planar resonator for efficient and accurate complex permittivity characterization of aqueous solutions," IEEE Trans. Microw. Theory Tech., vol. 61, no. 2, pp. 972-978, Feb. 2013.

[26] Keysight Technologies. (2009, Jan 1). Installation Guide, 85070/1E Dielectric Probe Kit and Materials Measurement Software [online]. Available: http://literature.cdn.keysight.com/litweb/pdf/85071-90010.pdf?id=535457

[27] M. Swithenbank et al., "On-Chip Terahertz-Frequency Measurement of Liquids," Analytical Chemistry, vol. 89, no. 15, pp. 7981–7987, Jul. 2017.

[28] Millimeter-Wave Technology & Solutions. Rectangular Waveguide Specification and MIL-Specification Cross Reference [online]. Available: http://www.millitech.com/pdfs/recspec.pdf

[29] D. M. Pozar, Microwave engineering, J. Wiley & Sons, Hoboken, 2012.

[30] Keysight Technologies. (2005, Sep 21). Free Space Materials Measurement Seminar [online]. Available: http://www.keysight.com/upload/cmc_upload/All/FreeSpaceSeminarRev2.pdf.

[31] Proceeding symposium IEEE/LEOS Benelux "A Quasi Optical Free Space Method"

[32] M.N. Afsar,"Complex Dielectric Measurement of Materials at Q-Band, V-Band and W-band Frequencies"

[33] "Development of Measurement and Extraction Technologies of Complex Permittivity Using Transmission Parameter", J. Inrared Milli Terahz Wave (2017)

[34] M. Halpern, H.P. Gush, E. Wishnow, and V. De Cosmo, "Far infrared transmission of dielectrics at cryogenic and room temperatures: glass, Fluorogold, Eccosorb, Stycast and various plastics," Appl. Opt., vol. 25, no. 4, pp.565-570, Feb. 1986.

[35] M. N. Afsar, "Precision millimeter-wave measurements of complex refractive index, complex dielectric permittivity, and loss tangent of common polymers" IEEE Trans. Instrum. Meas., vol. IM-36, no. 2, pp. 530-536, Jun. 1987.

[36] J. R. Birch, J. D. Dromey and J. Lesurf, "The optical constants of some common low-loss polymer between 4 – 40 cm^{-1}," Infrared Phys., vol. 21, pp. 225-228, 1981.

[37] Goodfellow. Technical Information – Polytetrafluoroethylene [online]. Available: http://www.goodfellow.com/catalogue/GFCat2H.php?ewd_token=fhGp0Xu0KcbmYhzaU3iRcK6gy9QQdr&n=Nh2YLW3z7J2NNkuXGR1ttVjEZl18Ts&ewd_urlNo=GFCat2L3&Head=FP30

[38] Goodfellow. Technical Information – Polyethylene – High density [online]. Available: http://www.goodfellow.com/catalogue/GFCat2H.php?ewd_token=d1MQ2bAax8GDdLEJhEY5CU4BGbZHur&n=otzexaQ9DPXWU3flmnj4GFBxlSJY74&ewd_urlNo=GFCat2L3&Head=ET32

[39] Goodfellow. Technical Information – Polymethylmethacrylate [online]. Available: http://www.goodfellow.com/catalogue/GFCat2H.php?ewd_token=d1MQ2bAax8GDdLEJhEY5CU4BGbZHur&n=otzexaQ9DPXWU3flmnj4GFBxlSJY74&ewd_urlNo=GFCat2L3&Head=ET32